IRANIAN JOURNAL OF CATALYSIS

CMCFO-Cr$_{0.1}$ Nanoferrites: Sol-gel Synthesis, Structural, and Magnetic Studies: Applications for Photodegradation of Congo Red Dye

Ahmed Selmi^{a*}, Hakimeh Teymourinia^{b,c,d}, Armin Zarei^{d}, Mohamed Timoumi^{e}, Ali Ramazani^{b,d*}

a) *Laboratory of Physical Chemistry of Materials, Faculty of Sciences of Monastir, University of Monastir, 5019 Monastir, Tunisia*

b) *Department of Biotechnology, Research Institute of Modern Biological Techniques (RIMBT), University of Zanjan, Zanjan 45371-38791, Iran*

c) *Trita Nanomedicine Research Center (TNRC), Zanjan Health Technology Park, Postal code 45156-13191, Zanjan, Iran*

d) *Department of Chemistry, Faculty of Science, University of Zanjan, 45371-38791 Zanjan, Iran*

e) *Laboratoire des Matériaux, Organisation et Propriétés, Faculté des Sciences de Tunis, Tunisia*

ABSTRACT

One of the foremost inescapable impediments that industrial sectors face is to remove organic pollutants, which affected nature and threatened the existence of species per se. Nanoscale magnetic ferrites are considerable materials for removing the majority of organic dyes due to their unique properties and high potential photocatalytic activity. Their photocatalytic performance in semiconductor nanocrystals has also received many enthusiasts over the last couple of years. Changing nanoferrites' architectural building blocks and increasing their bandgap energy may improve their photocatalytic peculiarities. In the present investigation, we have studied nanoscale magnetic ferrites with Co$_{0.4}$Mg$_{0.4}$Cu$_{0.2}$Fe$_{1.9}$Cr$_{0.1}$O$_4$, *(CMCFO-Cr$_x$, x= 0.1)* formula. *CMCFO-Cr$_x$* has synthesized via sol-gel approach. The synthesized nanoparticles were characterized by XRD, SEM, UV-vis analysis, and magnetic measurement, revealing the cubic spinel structure with space group Fd-3m (N° 277), average size between 20 and 60 nm, higher bandgap energy and saturation magnetization (446 emu/g) in the presence of transition metals. The results demonstrated in *CMCFO-Cr$_x$* (x=0.1) compound, the Curie temperature decreases to 446 K by the substitution of Fe^{3+} by Cr^{3+} ions. The synthesized powder nanoferrites efficiently degraded the Congo Red (CR) dye (84 %) under UV irradiation, for which the most probable degradation pathway is proposed. The recyclability test exhibited the nanoscale magnetic ferrites catalysts are sensibly efficient, stable, and facile recoverable by an external magnet. Thus, the *CMCFO-Cr$_x$* compounds can be an applicable catalyst in wastewater treatment.

Keywords: Nanoferrites, Characterization, Magnetic Measurement, Photocatalytic degradation, Congo Red (CR) dye.

1. Introduction

The world population is rapidly growing, and adequate supply of clean and fresh water is one of the great challenges to ensure the sustainable development of our society in the present century [1-3]. Currently, groundwater continuously contaminated with various organic pollutants, originating from various industries like textile, pharmaceutical, paper, cosmetic and painting, has been turned into one of the signifiant threats for the environment and especially for aquatic life [4].

The removal of these poisonous organic pollutants is of high importance and considered as an urgent phenomena as they are toxic, nonbiodegradable, and have a harmful impact on water [5-7]. So far, many efforts have been made to find suitable approaches to remove pollutants from wastewater [8-11].

In the procedure of organic dye pollutants removal, the photocatalytic procedure highly refers to adsorption process on the surface of the catalyst, meaning that higher adsorption sites lead to better photocatalytic performance [12, 13]. The organic dyes can be eliminated through a photocatalysis procedure in which photons' energy causes the excitation of the electron to higher conduction bnd, and finally forms photo-generated hole (h+), which can improve the catalytic

*Corresponding author:
E-mail address: *selmi.ahmed.fsg@gmail.com* (**A. Selmi**); aliramazani@gmail.com (**A. Ramazani**)

performance [14]. A cascade of reactions occur over the photocatalytic reactions:

i. Metal Oxide + hv → MO (h+ + e-)

ii. h+ + H$_2$O → H+ + OH•

iii. OH• + Organic dye →   CO$_2$ + H$_2$O (if degradation was complete)

Various oxides of nanomaterials have been evaluated as catalysts in the degradation process of many organic dyes such as methylene blue (MB), Congo Red (CR), and methyl orange (MO) [15]. Recently, Fallah Shojaei and co-workers prepared Metal-organic framework 5 (MOF-5) and bimetallic MOF-5s (Co/Zn and Ni/Zn) using a simple solvothermal for elimination of MB. The results revealed that

Co/Zn-MOF-5 showed a better photocalytic performance compared to those of Ni/Zn and raw MOF-5 because of its smaller size, the synergistic effect and the difference in the band gap [11]. Nezamzadeh-Ejhieh et al. synthesized coupled CdS-CuO nanoparticles (NPs) as powerful photocatalysts to remove MB, interestingly the coupled CdS-CuO NPs delineated the strongest photocatalytic activity (with excellent degradation of 98% during 120 min) in comparison with their monocomponent counterparts [4]. Coupled AgBr NPs to g-C3N4 were synthesized to obtain a catalyst for MO dye removal and bore excellent photocatalytic activities [16]. In another work, AFe$_2$O$_4$ (A: SR, Ca, and Ba) were utilized as a promising photocatalyst for CD dye removal under sunlight radiation and Xe lamp, postulating that BaF$_2$O$_4$ bore the highest degradation up to 92% after 75 min [17]. Iqbal's group has recently synthesized Cobalt ferrite (CoFe$_2$O$_4$) nanostructures using a simple and easy co-precipitation technique and tested their photocaralytic performance to eliminate CR dye. According to their final results, fs-CoFe$_2$O$_4$ nanostructure exhibited photodegradation ability (91%) [18].

The nanoscale magnetic ferrites have attracted great attention in the past decades because of temperature stability, permeability, high electrical resistivity, and magnetic properties [19], making them favorable for nanophotocatalysts and magnetic nanoadsorbents in the purification of wastewaters comprising inorganic and organic pollutants [20, 21]. Ferrites have a much higher degree of freedom to adapt substitution properties, which could make them a good candidate for photocatalytic degradation [22-24]. A ferrite spinel has the structural formula AB$_2$O$_4$, where A and B denote cations, which respectively occupy the tetrahedral site (Td) and the octahedral site (Oh). These A and B sites preferably occupied by cations such as rare earth or

alkaline earth elements and transition metals, which can give the compound excellent magnetic and catalytic properties due to the higher electron-hole pair generation rate of the nanopowder, providing a suitable environment for fast degradation of organic dye molecules. The incorporation of magnetic and non-magnetic ions such as transition metals and rare earth, induces various important properties of conductivity, photoluminescence, magnetic and photocatalytic field [25, 26]. According to the beneficial merits of magnetic nanoferrites, they can be a promising catalyst to remov organic dye pollutants from wastewaters. Herein, we have prepared a ferrite material substituted by chromium to test their catalytic activities for the elimination of CR dye under UV irridiation. A structural study wa undertaken to investigate the effect of substitution on the crystal cell and the magnetic properties of as-synthesized compound. The results demonstrated the synthesized nanomaterial is ecologically friendly, which has an important catalytic effect on the degradation of the Congo Red (CR) dye.

2.Experimental

2.1. Materials

Ferrite powders are prepared by the sol-gel auto-combustion method. Analytical grade Iron nitrate Fe(NO$_3$)$_3$.9H$_2$O, Nickel nitrate Ni(NO$_3$)$_2$.6H$_2$O, Zinc nitrate Zn(NO$_3$)$_2$.6H$_2$O Gadolinium nitrate Gd (NO$_3$)$_3$.6H$_2$O, Aluminium nitrate Al(NO$_3$)$_3$.6H$_2$O all with high purity (99%), ammonia solution NH$_4$OH, citric acid C$_6$H$_8$O$_7$.H$_2$O, ethylen-glycol C$_2$H$_6$O$_2$ Congo Red C$_{32}$H$_{22}$N$_6$Na$_2$O$_6$S$_2$.

2.2. Preparation of nanoferrites samples

A stoichiometric amount of metal nitrates that was proportional to the formula Co$_{0.4}$Mg$_{0.4}$Cu$_{0.2}$Fe$_{1.9}$Cr$_{0.1}$O$_4$ (*CMCFO-Cr$_{0.1}$*) was dissolved in 200 mL of deionized water. Then, citric acid and ethylene glycol were added to the solutio. The mixed solution heated up to 80 °C until the formation of the gel. The produced gel was transferred to an oven to 400°C. An auto-combustion reactio occurred leading to the formation of an aureate powder immediately. This powder was annealed at the following conditions: 400 °C for 6h, 600 °C for 8h, and 950 °C for 8h.

2.3. Characterization Methods

Structural analysis of the sample was carried out by X-ray diffraction technique with CuKα radiation (CuKα =1.5406 Å) in the range of 2θ-Theta: 10 - 70° with a step of 0.017°. Identification of the phases studied by use of X'Pert HightScore plus [27], and with the ICDD PDF-4

database. The morphology of nanoparticles was analyzed using scanning electron microscopy (SEM, Philips X130) under an accelerating voltage of 15 kV. Magnetic measurements were performed using a Vibrating Sample Magnetometer (VSM) with a cryogen-free Dynacool PPMS, operating at a vibration frequency of 40 Hz. The optical properties were recorded using UV–vis diffuse reflectance spectroscopy with a Perkin-Elmer Lambda 950 spectrophotometer at wavelengths ranging from 250 to 800 nm.

3. Results and Discussion

3.1. Structural properties

X-ray diffraction (XRD) analysis of the compound *CMCFO-Cr_{0.1}* was identified using the PDF-4 database, which confirms the cubic structure with the space group Fd-3m. **Fig. 1** shows the experimental and simulated XRD diffractogram. Degree of crystallinity is 78.73%. It should be noted that in comparison to the prepared prototypes ferrites compound, the size of the crystalline cell decreases. The size decreasing trend of the unit cell is attributed to the substitution of the larger ionic radius of Fe^{3+} (0.67 Å) by the ionic size of Cr^{3+} (0.64 Å) in the octahedral site [28]. The close ionic radii in divalent cations of A sites and trivalent cations of the B sites in tetrahedral and octahedral structures, respectively, are accommodating and the difference in the expansion of the tetrahedral and octahedral sites is characterized by a parameter called oxygen parameter or anion parameter (u). The difference in the expansion of the tetrahedral and octahedral sites is characterized by a parameter called oxygen parameter or anion parameter (*u*). The oxygen parameter (*u*) is a quantity that represents the shifting of oxygen ions due to the substitution of cation at the tetrahedral (A) site. As (*u*) increases, oxygen ions shift in such a way that the distance between A and O ions (R_A) is increased while that the distance between B and O ions (R_B) is decreased, and when the (*u*) parameter decreases, the O ions are displaced in such a way that R_A decreases and R_B increases. In all ideal spinels, the parameter u has a value in the neighborhood of 0.375 (*u* = 3/8). However, in the actual spinel lattice, this ideal pattern is slightly deformed and usually corresponds to u > 0.375 [29]. The theoretical lattice constant (a_{th}), is calculated based on the cation distribution with the following relation:

$$a = \frac{\lambda}{2}\frac{\sqrt{h^2+l^2+k^2}}{sin\theta} \qquad Eq.\ (1)$$

λ *the* wavelength of the copper radiation ($\lambda_{CuK\alpha}$=1.54056 Å) and θ is the Bragg angle corresponding to the most intense Miller indices (hkl) which in this case is (311).

The average crystallite size (L) was calculated from the (311) from the width of the maximum diffraction limits using the empirical formula of Debye-Scherrer [30, 31].

$$L = \frac{k\ \lambda}{\beta\ cos\theta} \qquad Eq\ (2)$$

Where *k = 0.89* (assuming the particles are spherical); λ is the wavelength of X-ray diffraction; β is the full width at half maximum (FWHM of the diffraction peak; and θ the angle of diffraction.

The Williamson-Hall equation is used to calculate the crystallite size.

$$\beta\ Cos\theta =\ K\ \lambda/D + C.e.Sin\theta \qquad Eq.\ (3)$$

Where β is the full width of the Bragg peak at half maximum (FWHM), θ is peak angle, D is mean crystallite size, e is strain and K~1 [32].

The results of Rietveld refinement, the degree of crystallinity, and the size of crystallites are summarized in **Table 1**. **Table. 1** comprising the results of Rietveld refined cell parameters (Å), R-factor values, degree of crystallinity, which was simulated using the ReaxFF program [33], and nanoparticles size which were calculated from the highest peak in the XRD diffractogram and SEM images (**Fig. 2**). Average size of *CMCFO-Cr_{0.1}* nanoparticles from XRD and SEM is 16 nm and 57 nm, respectively, showing a significant difference between them. The particle size calculated by SEM analysis, in reality, represents the size of an agglomeration grains, which is formed from several nanocrystallites [34]. In addition, SEM image shows that the morphology of the obtained *CMCFO-Cr_{0.1}* nanoparticles is also in the form of a cauliflower. *CMCFO-Cr_{0.1}* nanoparticles formed in irregularly shapes and non-uniform particles with average size between 20-60 nm.

3.2. Magnetic properties

CoFe₂O₄ (Cobalt ferrite) is of high important magnetic nanoparticles (NPs) bearing supreme peculiarities e.g., high cubic magnetic crystalline anisotropic, narrow bandgap, high correctivity, and high curie temperature [35-37]. It is worthy pointing out that Cobat ferrite NPs intercalation can improve the efficiency, facilitate the separation after completion photodegradation process, and will enhance absorption in visible light area [38, 39]. Cobalt ferrites pose a high curie temperature which makes them applicable, separable, and recyclable even in a wide range of high temperatures [37].

The temperature (T) dependence on magnetization (M) reveals that *CMCFO-Cr_{0.1}* has a magnetic transition
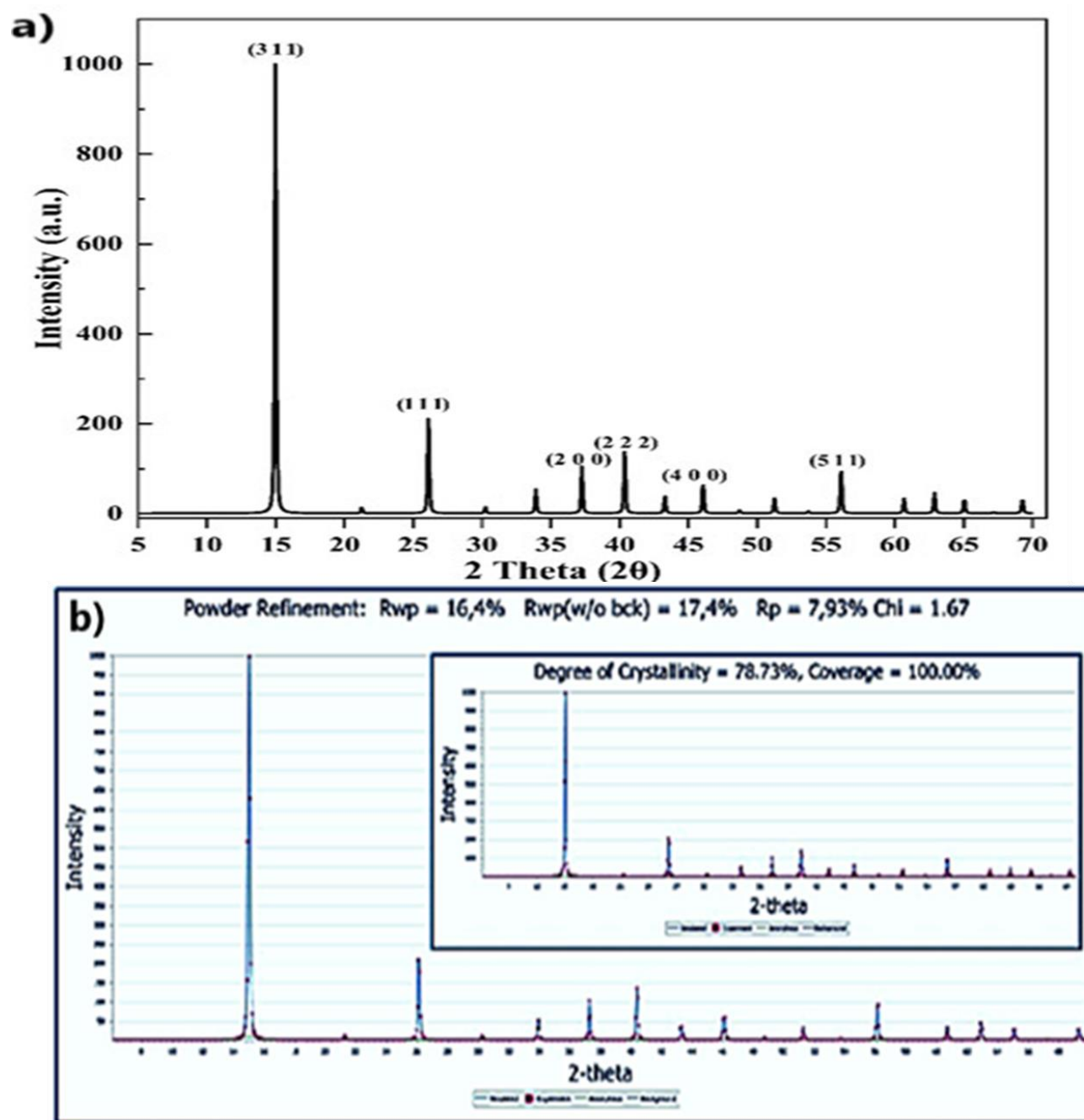
Figure 1. a) XRD pattern and b) The simulated degree of crystallinity of *CMCFO-Cr$_x$ (x=0.1)* nanoferrites

Table. 1. Rietveld refined cell parameters (Å), R-factor values, degree of crystallinity, and nanoparticles size of Co$_{0.4}$Mg$_{0.4}$Cu$_{0.2}$Fe$_{1.9}$Cr$_{0.1}$O$_4$.

Sample	Co$_{0.4}$Mg$_{0.4}$Cu$_{0.2}$Fe$_{1.9}$Cr$_{0.1}$O$_4$
	(CMCFO-Cr$_{0.1}$)
Space group	Fd-3m
Cell parameters	8.345(4)
R-Factors	7.93
R$_P$ (%)	17.4
R$_{WP}$ (%)	16.4

χ^2	1.67
Degree of crystallinity (%)	78.73
* Nanoparticles size (nm)	
	16
- Debye-Scherrer	21
-Williamson-Hall	
- SEM	57
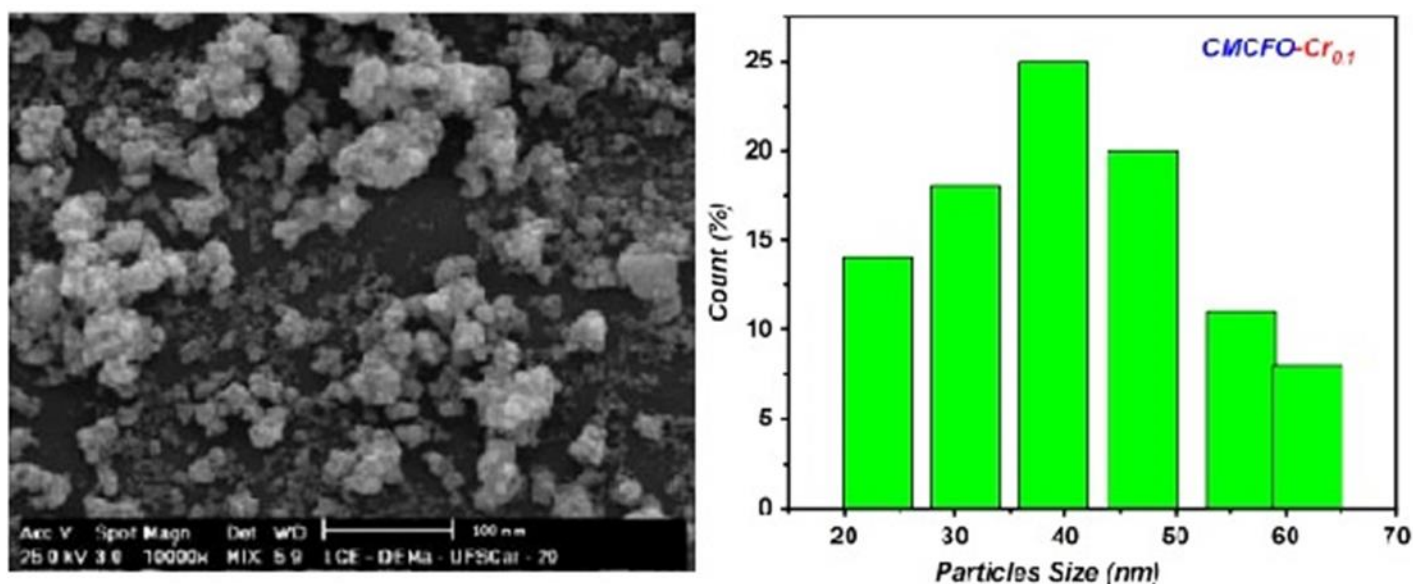
Figure 2. a) SEM image and b) grain size distribution of prepared *CMCFO-Cr$_x$ (x=0.1)* nanoferrites.

from a ferromagnetic (FM) state to a paramagnetic (PM) transition state at Curie temperature (T_C = 376 K). The evolution of the magnetization M and dM/dT versus the temperature (T) shown in the inset of **Fig. 3a**.

Analysis of the compounds that belong to the same spinel family reveals a decrease in the curie temperature Tc with the substitution of the Fe^{3+} ions by Cr^{3+} in the (B) site and these are explained by the difference between the magnetic elements of them ($\mu_{eff}(Fe^{3+})$ = 5.36 MB and $\mu_{eff}(Cr^{3+})$ = 3.85 MB). The decrease in magnetic moments induces a decrease in the magnetization between the two sub-lattice A and B of the spinel AB_2O_4 [40].

In **Table 2**, the Curie temperatures Tc of certain AB_2O_4 type ferrite compounds were depicted together in the cited table. Analysis of the mentioned results in the table

shows clearly that when the amount of substitution in the octahedral site (B) increase, the Curie temperature decreases, these results are located for compounds of general formula $MFe_{2-x}Cr_xO_4$, it is well known that the Curie temperature is also related to the ions in the tetrahedral sites (A) [41, 42].

3.3. Photocatalytic degradation of Congo red (CR) by nanoferrites

Several studies have been carried out previously to study the effect of pH on the degradation of Congo Red. Studies reveal that the pH range between 4- 8 is useful for photodegradation [43, 44], therefore, all the experiments are carried out at a pH approximately equal to 8. **Table 3** demonstrates the summary of some physicochemical characteristics of Congo Red.

3.3.1 Effect of light on photodegradation

The photocatalytic properties of the prepared nanoferrites were investigated for the degradation of
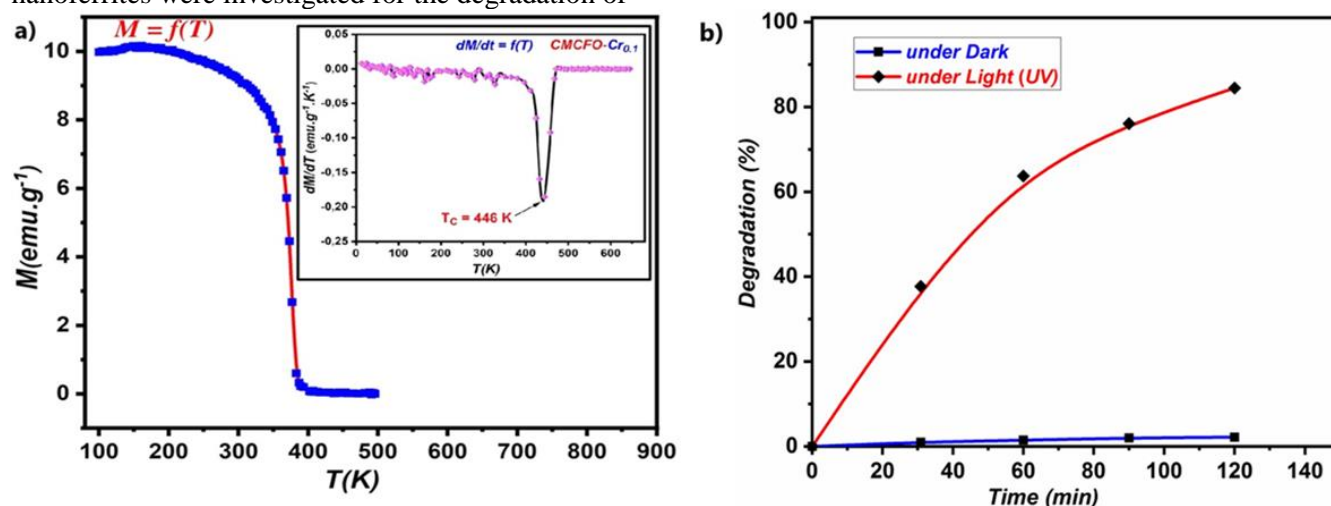
Figure 3. a) M- T curves of the nanoferrites compound (*CMCFO-Cr*). Inset: Plot of dM/dT versus T. **b)** Plot of the CR dye degradation percent versus Time in the presence of prepared chromium substituted ferrite *CMCFO-Cr* under the dark and UV light.

Table. 2. Curie temperature of Cr-substituted ferrite nanomaterials.

Chemical formula	Tc (K)	References
* $Mg_{1-x}Co_xCr_xFe_{2-x}O4$ (0≤x≤0.5)		[30]
x=0		
x=0.1	681	
x=0.2	727	
x=0.3	766	
x=0.4	682	
x=0.5	660	
*$Zn_{0.54}Co_{0.46}Cr_xFe_{2-x}O_4$ (0.45≤x≤0.75)	618	
x=0.45	375	
x=0.55	353	[31]
x=0.65	329	
x=0.70	310	
x=0.75	301	

organic pollutions such as Congo Red (CR) dye. The percentage of degradation of CR dye was studied under UV light and darkness. For this purpose, 10 mg of the catalyst was dissolved in a 200 ml solution containing the 30 mg of CR. **Fig. 3b**., this demonstrates the percentage of degradation of the CR dye under UV light and darkness. The following equation is used to calculate the percent of photocatalytic degradation of CR dye:

$$Degradation\ rate\ (\%) = \frac{100\ (A_0 - A_t)}{A_0} \qquad Eq.\ (3)$$

Where A_0 is initial absorbance and A_t is the absorbance after a period of a time *t*.

3.3.2 Influence of catalyst dose on the photocatalytic degradation of CR dye

To evaluate the effect of catalyst dose, five solutions containing 0.01 to 0.05 g/L of catalyst were

investigated. All solutions were prepared using 2 g of CR dye in 200 ml of deionized water, which wa made by treating for 30 min in the dark. Then, UV-Vis analysis was done for each solution to measure the absorbance and deduced the percentage of degradation. **Fig. 4a**. shows that the amount of

Table. 3. Summary of some physicochemical characteristics of Congo Red.

Congo Red Properties	Figure
Melting point: >360 °C (lit.) Density : 0.995 g/mL at 25 °C Solubility Water: 10mg/mL Powder : Solid Color Red Brown pH 6.7 (10g/l, H_2O, 20℃) λ_{max}: 497nm Major Application and danger : Textile, fertilizer, pesticides, carbohydrates, treatment of pathogen infections, age-related macular degeneration. Detecting bacteria, protein folding disorders; treating dermatological disorders, neurodegenerative diseases, Alzheimer's disease	
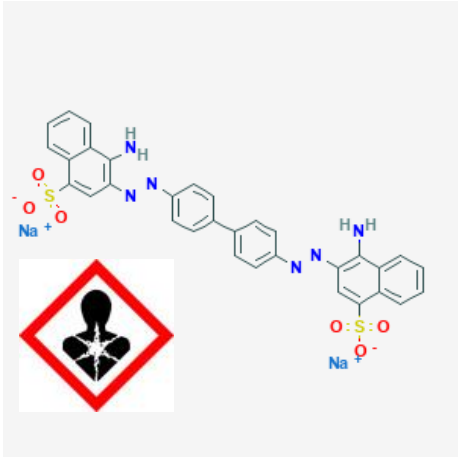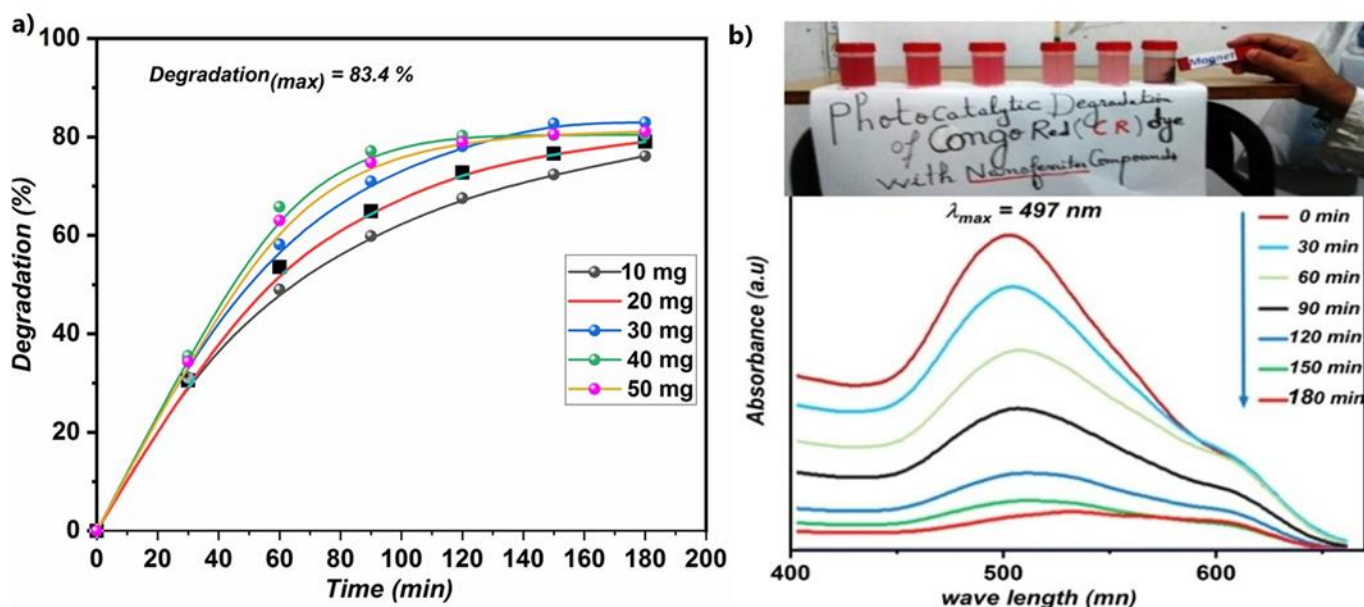
Figure 4. a) The effect of *CMCFO-Cr* catalysts amounts towards the degradation of the Congo Red dye **b)** Absorption spectra of CR dye solutions under visible light radiation (Reaction conditions: 2g CR dye/200mL, catalyst amount = 0.03 g/L, pH=natural and room temperature).

degradation is directly related to the amount of catalyst. It is clear that the amount of degradation exposed to UV light is significantly greater than the amount of damage in the dark. This process is related to the photocatalytic reactions of the prepared nanoferrites, for which the mechanism of degradation is described below.

3.3.3 Influence of irradiation time on the photocatalytic degradation of CR dye

The irradiation time plays a key role in the photocatalytic process. In this work, six solutions of 0.03 g/L of catalyst and 2 mg of CR in 200 ml of distilled water were prepared. The solutions were under the

irradiation of UV lamp and the sampling was performed every 30 minutes for UV-Vis analysis. The UV-Vis curves indicate the maximum degradation was reached after 150 min. The advantage of The nanoferrites catalysts bear sustainable benefits e.g., they are easily recoverable using a magnet (**Fig. 4b**), and are reusable via high temperature treatment (around 200 °C) to the decomposition of the organic species [45].

3.3.4 Proposed photocatalysis mechanism

The conduction band electrons (e-) and valence band holes (h^+) are generated when photocatalyst powders suspended in an aqueous solution are irradiated with light having energy equal to or higher than its bandgap energy. The photogenerated electrons can both reduce the dissolved organic dye molecules and react with electron acceptors, such as O_2 adsorbed on the photocatalyst surface or dissolved in water, leading to its reduction to superoxide radical anion, $O_2^{\cdot}$. The photogenerated holes can both oxidize the organic dye molecules to form oxidized species and react with OH or H_2O, leading to their transformation to hydroxyl radical, $OH^{\cdot}$. The resulting $O_2^{\cdot}$ and $OH^{\cdot}$ radicals are reported to play a significant role in the photocatalytic degradation of azo dye molecules. The possible reactions occurring at the nanoferrites semiconductor photocatalyst surface to result from photocatalytic oxidation can be expressed as follows [46-49]:

$Co_{0.4}Mg_{0.4}Cu_{0.2}Fe_{1.9}Cr_{0.1}O_4$ + hv ¾¾®; $Co_{0.4}Mg_{0.4}Cu_{0.2}Fe_{1.9}Cr_{0.1}O_4^{\cdot} + (é + h^+)$
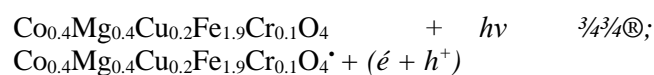
The photo-generated holes created in the valence band readily oxidize with H_2O or OH^- species from the surrounding environment to form. OH, radicals. hv also acts as an oxidant via direct organic contaminant degradation depending on the catalyst type and oxidative surroundings

$h^+ + H_2O$ ¾¾®; $OH^{\cdot} + H^+$
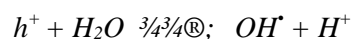
Similarly, the electron in the valence band reacts with the adsorptive oxygen on the surface of nanoparticles to produce anionic superoxide species ($O_2^{\cdot}$) via reduction, which later reacts with hv or H_2O to form

$é + O_2$ ¾¾®; O_2^-

$OH^{\cdot} + O_2- + CR\ dye$ ¾¾®; Degradation of the dye
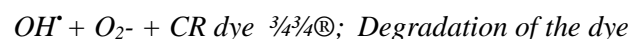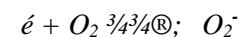
The $O_2^{\cdot}$ and $OH^{\cdot}$ as well as $HO_2^{\cdot}$ radicals which formed subsequently, possess an extremely strong oxidizing power and can oxidize most of the azo dye molecules to less harmful products, such as H_2O and CO_2. By this means, most azo dyes that are intrinsically reactive toward hydroxyl radicals can be degraded via photocatalysts, which are greatly affected by the valence band edge position of semiconductive photocatalysts. The reduction in photocatalyst is also involved in the azo dye degradation, but less than the oxidation pathway [50].

4. Conclusions

The chromium substituted nanoferrites with $Co_{0.4}Mg_{0.4}Cu_{0.2}Fe_{1.9}Cr_{0.1}O_4$, (CMCFO-Cr$_x$, x= 0.1) formula were successfully synthesized by sol- gel methods with average crystallite size of 57 nm. Magnetic investigation proves that the Curie temperature decreases with the substitution of Fe^{3+} ions by Cr^{3+} in the octahedral site (B). The catalytic degradation of Congo red (CR) dye using nanoferrites as a catalyst was studied. Results showed the photocatalytic efficiency of the *CMCFO-Cr$_{0.1}$* nanoferrites improved when the aqueous solutions of the mixture were irradiated with UV light, which also accelerates the oxidation processes. High photocatalytic efficiency of as-prepared CMCFO-Cr0.1 nanoferrites degraded almost 84% of CR. The novelty of this type of catalyst also lies in the fact that hybrid nanomaterials allow its use as a degreaser also under light conditions. This characteristic would be rather advantageous for applications of the catalyst.

Conflicts of interest

The authors declare no competing interests.

Ethics approval

All authors approved.

Consent to participate (authors' contributions)

All authors participated.

References

[1]. Jabbari, R. and N. Ghasemi, Investigating Methylene Blue Dye Adsorption Isotherms Using Silver Nano Particles Provided by Aqueous Extract of Tragopogon Buphthalmoides, Chem. Methodolog. 2021. 5(1): p. 21-29.

[2]. Tesh, S.J. and T.B. Scott, Nano-composites for water remediation: A review Adv. Mater. 2014. 26(35): p. 6056-6068.

[3]. Teymourinia, H., et al., Synthesis of graphene quantum dots from corn powder and their application in reduce charge recombination and increase free charge carriers J. Mol. Liq. 2017. 242: p. 447-455.

[4]. Senobari, S. and A. Nezamzadeh-Ejhieh, A comprehensive study on the photocatalytic activity of coupled copper oxide-cadmium sulfide nanoparticles Spectrochimica Acta Part A: Mol. Biomol. Spec. 2018. 196: p. 334-343.

[5]. Ling, S.K., S. Wang, and Y. Peng, Oxidative degradation of dyes in water using Co2+/H2O2 and Co2+/peroxymonosulfate J. Hazard. Mater. 2010. 178(1-3): p. 385-389.

[6]. Rasouli, N., et al., An insight on kinetic adsorption of Congo red dye from aqueous solution using magnetic chitosan based composites as adsorbent Chem. Methodolog. 2017. 1(1): p. 74-86.

[7]. Salavati, H., A. Teimouri, and S. Kazemi, Synthesis and characterization of novel composite-based phthalocyanine used as efficient photocatalyst for the degradation of methyl orange, Chem. Methodolog. 2017. 1(1): p. 12-27.

[8]. Alidadykhoh, M., H. Pyman, and H. Roshanfekr, Application of a new polymer AgCl nanoparticles coated polyethylene terephetalat [PET] as adsorbent for removal and electrochemical determination of methylene blue dye, Chem. Methodolog. 2021. 5(2): p. 96-106.

[9]. Amar, I., et al., Removal of methylene blue from aqueous solutions using nano-magnetic adsorbent based on zinc-doped cobalt ferrite, Chem. Methodolog. 2020. 4(1): p. 1-18.

[10]. Ranjbar, S., G. Haghdoost, and A. Ebadi, Adsorption of Methyl Red Dye from Aqueous Solution Using Gamma Alumina Nanoparticles Chem. Methodolog. 5(2): p. 190-199.

[11]. Zebardast, M., A. Fallah Shojaei, and K. Tabatabaeian, Enhanced removal of methylene blue dye by bimetallic nano-sized MOF-5s Iran. J. Catal. 2018. 8(4): p. 297-309.

[12]. Bekkali, C.E., et al., Effects of metal oxide catalysts on the photodegradation of antibiotics effluent, Iran. J. Catal. 2018. 8(4): p. 241-247.

[13]. Sadeghi, M., M. Irandoust, and H. Azadi, Efficient photocatalytic decolorization of methylene blue and victoria blue using reusable TiO2 magnetic nanocomposite modified with zinc under UV irradiation: optimization via response surface methodology (RSM) Desalination and Water Treatment 2018. 114: p. 285-296.

[14]. Casbeer, E., V.K. Sharma, and X.-Z. Li, Synthesis and photocatalytic activity of ferrites under visible light: a review, Separat. Purif. Tech. 2012. 87: p. 1-14.

[15]. Viswanathan, B., Photocatalytic degradation of dyes: an overview, Current Catal. 2018. 7(2): p. 99-121.

[16]. Ghattavi, S. and A. Nezamzadeh-Ejhieh, GC-MASS detection of methyl orange degradation intermediates by AgBr/g-C3N4: Experimental design, bandgap study, and characterization of the catalyst Inter. J. Hydrogen Ener. 2020. 45(46): p. 24636-24656.

[17]. Vijayaraghavan, T., et al., Rapid and efficient visible light photocatalytic dye degradation using AFe2O4 (A= Ba, Ca and Sr) complex oxides, Mater. Sci. Eng.: B 2016. 210: p. 43-50.

[18]. Ali, N., et al., Photocatalytic degradation of congo red dye from aqueous environment using cobalt ferrite nanostructures: development, characterization, and photocatalytic performance Water, Air, & Soil Pollution 2020. 231(2): p. 1-16.

[19]. Zarei, A. and S. Saedi, Synthesis and application of Fe 3 O 4@ SiO 2@ Carboxyl-terminated PAMAM Dendrimer Nanocomposite for heavy metal removal, J. Inorganic Organometal. Poly. Mater. 2018. 28(6): p. 2835-2843.

[20]. Abbas, N., et al., The photocatalytic performance and structural characteristics of nickel cobalt ferrite nanocomposites after doping with bismuth, J. Colloid Interf. Sci. 2021. 594: p. 902-913.

[21]. Behura, R., R. Sakthivel, and N. Das, Synthesis of cobalt ferrite nanoparticles from waste iron ore tailings and spent lithium ion batteries for photo/sono-catalytic degradation of Congo red, Powder Tech. 2021. 386: p. 519-527.

[22]. Ichimura, T., K. Fujiwara, and H. Tanaka, Dual field effects in electrolyte-gated spinel ferrite: electrostatic carrier doping and redox reactions, Sci. reports 2014. 4(1): p. 1-5.

[23]. Liu, S.-Q., Magnetic semiconductor nano-photocatalysts for the degradation of organic pollutants Environ. Chem. Lett. 2012. 10(3): p. 209-216.

[24]. Shobana, M., Nanoferrites in biosensors–A review Mater. Sci. Eng. B 2021. 272: p. 115344.

[25]. Iqbal, M.A., et al., La-and Mn-codoped Bismuth Ferrite/Ti3C2 MXene composites for efficient photocatalytic degradation of Congo Red dye ACS Omega 2019. 4(5): p. 8661-8668.

[26]. Noack, C.W., D.A. Dzombak, and A.K. Karamalidis, Rare earth element distributions and trends in natural waters with a focus on groundwater, Environ. Sci. Tech. 2014. 48(8): p. 4317-4326.

[27]. Degen, T., et al., The highscore suite Powder Diffraction 2014. 29(S2): p. S13-S18.

[28]. Thankachan, R.M., et al., Cr 3+-substitution induced structural reconfigurations in the nanocrystalline spinel compound ZnFe 2 O 4 as revealed from X-ray diffraction, positron annihilation and Mössbauer spectroscopic studies RSC Adv. 2015. 5(80): p. 64966-64975.

[29]. Shelke, S.B., Studies on the Structural, Electrical and Magnetic Properties of Some Substituted Spinel Ferrites. Insta Publishing. 2020, P. 1-7.

[30]. Holzwarth, U. and N. Gibson, The Scherrer equation versus the'Debye-Scherrer equation' Nature Nanotech 2011. 6(9): p. 534-534.

[31]. Teymourinia, H., et al., Application of green synthesized TiO2/Sb2S3/GQDs nanocomposite as high efficient antibacterial agent against E. coli and Staphylococcus aureus, Mater. Sci. Eng.: C 2019. 99: p. 296-303.

[32]. Yaghoubi-berijani, M., B. Bahramian, and S. Zargari, The Study of Photocatalytic Degradation Mechanism under Visible Light Irradiation on BiOBr/Ag Nanocomposite, Iran. J. Catal. 2020. 10(4): p. 307-317.

[33]. Senftle, T.P., et al., The ReaxFF reactive force-field: development, applications and future directions npj Computational Materials 2016. 2(1): p. 1-14.

[34]. Pubby, K., et al., Cobalt substituted nickel ferrites via Pechini's sol–gel citrate route: X-band electromagnetic characterization, J. Magnetism Magnetic Mater. 2018. 466: p. 430-445.

[35]. Houshiar, M., et al., Synthesis of cobalt ferrite (CoFe2O4) nanoparticles using combustion, coprecipitation, and precipitation methods: A comparison study of size, structural, and magnetic properties J. Magnetism Magnetic Mater. 2014. 371: p. 43-48.

[36]. Toksha, B., et al., Structural investigations and magnetic properties of cobalt ferrite nanoparticles prepared by sol–gel auto combustion method, Solid State Commun. 2008. 147(11-12): p. 479-483.

[37]. Wilson, A., et al., Preparation and photocatalytic properties of hybrid core–shell reusable CoFe2O4–ZnO nanospheres J. Magnetism Magnetic Mater. 2012. 324(17): p. 2597-2601.

[38]. Ferdosi, E., H. Bahiraei, and D. Ghanbari, Investigation the photocatalytic activity of CoFe2O4/ZnO and CoFe2O4/ZnO/Ag nanocomposites for purification of dye pollutants Separation and Purification Technology 2019. 211: p. 35-39.

[39]. Sathishkumar, P., et al., ZnO supported CoFe2O4 nanophotocatalysts for the mineralization of Direct Blue 71 in aqueous environments J. Hazard. Mater. 2013. 252: p. 171-179.

[40]. Wahba, A.M. and M.B. Mohamed, Structural, magnetic, and dielectric properties of nanocrystalline Cr-substituted Co0. 8Ni0. 2Fe2O4 ferrit, Ceramics Inter. 2014. 40(4): p. 6127-6135.

[41]. Bugarčić, M., et al., Vermiculite enriched by Fe (III) oxides as a novel adsorbent for toxic metals removal J. Environmen. Chem. Eng. 2021. 9(5): p. 106020.

[42]. Jasrotia, R., et al., Photocatalytic degradation of environmental pollutant using nickel and cerium ions substituted Co 0.6 Zn 0.4 Fe 2 O 4 nanoferrites Earth Systems and Environment 2021: p. 1-19.

[43]. Boutra, B., et al., Magnetically separable MnFe2O4/TA/ZnO nanocomposites for photocatalytic degradation of Congo Red under visible light J. Magnetism Magnetic Mater. 2020. 497: p. 165994.

[44]. Rahimi, R., et al., Synthesis, characterization and adsorbing properties of hollow Zn-Fe2O4 nanospheres on removal of Congo red from aqueous solution Desalination 2011. 280(1-3): p. 412-418.

[45]. Hezam, F., O. Nur, and M. Mustafa, Synthesis, structural, optical and magnetic properties of NiFe2O4/MWCNTs/ZnO hybrid nanocomposite for solar radiation driven photocatalytic degradation and magnetic separation Colloids and Surfaces A: Physicochemical and Engineering Aspects 2020. 592: p. 124586.

[46]. Bianco Prevot, A., et al., Photocatalytic degradation of acid blue 80 in aqueous solutions containing TiO2 suspensions Environ. Sci. Tech. 2001. 35(5): p. 971-976.

[47]. Houas, A., et al., Photocatalytic degradation pathway of methylene blue in water Appl. Catal. B: Environ. 2001. 31(2): p. 145-157.

[48]. Riga, A., et al., Effect of system parameters and of inorganic salts on the decolorization and degradation of Procion H-exl dyes. Comparison of H2O2/UV, Fenton, UV/Fenton, TiO2/UV and TiO2/UV/H2O2 processes Desalination 2007. 211(1-3): p. 72-86.

[49]. Teymourinia, H., et al., GQDs/Sb2S3/TiO2 as a co-sensitized in DSSs: improve the power conversion efficiency of DSSs through increasing light harvesting by using as-synthesized nanocomposite and mirror Appl. Surf. Sci. 2020. 512: p. 145638.

[50]. Vinodgopal, K., et al., A photocatalytic approach for the reductive decolorization of textile azo dyes in colloidal semiconductor suspensions Langmuir 1994. 10(6): p. 1767-1771.